A Ca$_V$β SH3/Guanylate Kinase Domain Interaction Regulates Multiple Properties of Voltage-gated Ca^{2+} Channels

Shoji X. Takahashi, Jayalakshmi Miriyala, Lai Hock Tay, David T. Yue, and Henry M. Colecraft

Calcium Signals Laboratory, Department of Biomedical Engineering, Johns Hopkins University School of Medicine, Baltimore, MD 21205

Auxiliary Ca^{2+} channel β subunits (Ca$_V$β) regulate cellular Ca^{2+} signaling by trafficking pore-forming α$_1$ subunits to the membrane and normalizing channel gating. These effects are mediated through a characteristic *src* homology 3/ guanylate kinase (SH3–GK) structural module, a design feature shared in common with the membrane-associated guanylate kinase (MAGUK) family of scaffold proteins. However, the mechanisms by which the Ca$_V$β SH3–GK module regulates multiple Ca^{2+} channel functions are not well understood. Here, using a split-domain approach, we investigated the role of the interrelationship between Ca$_V$β SH3 and GK domains in defining channel properties. The studies build upon a previously identified split-domain pair that displays a trans SH3–GK interaction, and fully reconstitutes Ca$_V$β effects on channel trafficking, activation gating, and increased open probability (P_o). Here, by varying the precise locations used to separate SH3 and GK domains and monitoring subsequent SH3–GK interactions by fluorescence resonance energy transfer (FRET), we identified a particular split-domain pair that displayed a subtly altered configuration of the trans SH3–GK interaction. Remarkably, this pair discriminated between Ca$_V$β trafficking and gating properties: α$_{1C}$ targeting to the membrane was fully reconstituted, whereas shifts in activation gating and increased P_o functions were selectively lost. A more extreme case, in which the trans SH3–GK interaction was selectively ablated, yielded a split-domain pair that could reconstitute neither the trafficking nor gating-modulation functions, even though both moieties could independently engage their respective binding sites on the α$_{1C}$ (Ca$_V$1.2) subunit. The results reveal that Ca$_V$β SH3 and GK domains function codependently to tune Ca^{2+} channel trafficking and gating properties, and suggest new paradigms for physiological and therapeutic regulation of Ca^{2+} channel activity.

INTRODUCTION

High voltage–activated calcium channels, comprised of pore-forming (α$_1$) and auxiliary (α$_2$δ, Ca$_V$β, and sometimes γ) subunits, transduce electrical signals into Ca^{2+} fluxes that regulate essential biological processes such as neurotransmission, muscle contraction, and gene expression (Tsien and Tsien, 1990; Catterall, 2000). Auxiliary Ca$_V$β subunits (Ca$_V$β$_1$–Ca$_V$β$_4$) exert a powerful influence on cellular Ca^{2+} signaling by regulating multiple functional properties of α$_1$ subunits (α$_{1A}$–α$_{1F}$, α$_{1S}$; Ca$_V$1.1–1.4, Ca$_V$2.1–2.3) (Ertel et al., 2000), including trafficking the channel complex to the plasma membrane (Chien et al., 1995; Brice et al., 1997; Gao et al., 1999), producing hyperpolarizing shifts in the voltage dependence of channel activation (Singer et al., 1991; Perez-Reyes et al., 1992; De Waard et al., 1994), increasing channel open probability (P_o) (Gerster et al., 1999; Hullin et al., 2003), and producing characteristic effects on the rate of channel inactivation (Wei et al., 2000; Stotz and Zamponi, 2001; Colecraft et al., 2002; Dolphin, 2003; Takahashi et al., 2003). Unraveling how Ca$_V$βs regulate these myriad effects is fundamental to understanding the operation of Ca^{2+} channels in both physiological and disease states, as well as to efforts to

target the α$_1$–β interaction to generate a new class of therapeutically useful Ca^{2+} channel inhibitors (Young et al., 1998). Nevertheless, mechanistic understanding of how Ca$_V$βs regulate multiple Ca^{2+} channel properties is lacking, despite years of intense research focus. One ambiguous area is how structural determinants on Ca$_V$β combine to regulate multiple functional properties of α$_1$ subunits. Fortunately, recent high resolution crystal structures of Ca$_V$βs (Chen et al., 2004; Opatowsky et al., 2004; Van Petegem et al., 2004) provide new opportunities for increased mechanistic understanding of how Ca$_V$βs tune Ca^{2+} channel behavior.

The Ca$_V$β crystal structures directly reveal *src* homology 3 (SH3) and guanylate kinase-like (GK) motifs within two domains conserved among distinct Ca$_V$β isoforms (C1 and C2; Fig. 1, A and B) (De Waard et al., 1994; Birnbaumer et al., 1998). These structural features establish a link between Ca$_V$βs and the membrane-associated guanylate kinase (MAGUK) family proteins that play a vital role in organizing intracellular signaling

---

Correspondence to Henry M. Colecraft: hcolecr1@jhmi.edu

Abbreviations used in this paper: AID, α1 interaction domain; Ca$_V$β, Ca^{2+} channel β subunit; CFP, cyan fluorescent protein; *FR*, FRET ratio; FRET, fluorescence resonance energy transfer; GK, guanylate kinase; MAGUK, membrane-associated guanylate kinase; P_o, open probability; SH3, *src* homology 3; YFP, yellow fluorescent protein.

pathways; SH3–GK is an essential functional module conserved among MAGUKs (Anderson, 1996; Craven and Bredt, 1998). The $Ca_V\beta$ SH3–GK core is sufficient to reconstitute the bulk of $Ca_V\beta$ functional effects, including promoting membrane transport of pore-forming α_1 subunits (Gao et al., 1999) and robustly increasing recombinant whole-cell Ca^{2+} channel currents when coexpressed with α_1 (Opatowsky et al., 2003). Therefore, this structural unit holds the key for mechanistic insights into how the α_1–β interaction regulates multiple channel properties.

How does the two-pronged nature of the SH3–GK module impact functional operation of $Ca_V\beta$s? For nearly a decade, it was believed that the second conserved domain of $Ca_V\beta$ (C2), now known to constitute a GK domain, was primarily responsible for channel regulation (De Waard et al., 1994; Walker and De Waard, 1998). Consistent with this idea, high-resolution crystal structures of $Ca_V\beta$ subunits in complex with a conserved α_1 interaction domain (AID) peptide, indicate that the AID interacts exclusively with the GK domain (Chen et al., 2004; Opatowsky et al., 2004; Van Petegem et al., 2004). However, recent functional experiments implicate a more prominent role for the SH3 domain than previously suspected (Opatowsky et al., 2003; Takahashi et al., 2004; Yue, 2004; Maltez et al., 2005). Specifically, using a split-domain approach, we (Takahashi et al., 2004) showed that $Ca_V\beta_{2a}$ fragments containing either the SH3 (NSH3) or GK (GKC) domains (Fig. 1 C) reconstituted wild-type $Ca_V\beta$ function only when both fragments were coexpressed with recombinant α_{1C} in HEK 293 cells. Qualitatively similar results were obtained for split-domain $Ca_V\beta$ regulation of $Ca_V2.1$ and $Ca_V1.2$ in *Xenopus* oocytes (Opatowsky et al., 2003; Maltez et al., 2005). The unexpected importance of the $Ca_V\beta$–SH3 domain in Ca^{2+} channel modulation raises new questions regarding how structural determinants on $Ca_V\beta$ cooperate to regulate channel properties. Do SH3 and GK domains act independently to reconstitute $Ca_V\beta$ functions, or does the SH3 domain act allosterically via interaction with GK? Is the $Ca_V\beta$ SH3–GK interaction necessary for channel modulation? Does $Ca_V\beta$ SH3 domain bind independently to the α_1 subunit?

Here, we combine a split-domain approach with site-directed mutagenesis, electrophysiology, and FRET determination of protein interactions to investigate these issues. We find that the configuration of the SH3–GK interaction is a dominant determinant of $Ca_V\beta$ function. Subtle changes in the relative affinity and orientation of the $Ca_V\beta$ SH3–GK domain interaction produces significant effects on channel properties by preferentially preventing the increased-P_o and shift in activation gating functions, whereas the channel trafficking role is retained. Moreover, selectively ablating the SH3–GK in-

teraction disrupted both trafficking and gating modulation, indicating that the two motifs act codependently to reconstitute $Ca_V\beta$ function. The results shed new light on how the structural design of $Ca_V\beta$s relates to their regulation of multiple Ca^{2+} channel functions, and reveal an unexpected signaling versatility of the SH3–GK module.

MATERIALS AND METHODS

DNA Cloning
α_{1C}-GFP was described previously (Takahashi et al., 2004). Split-domain β_{2a} constructs (NSH3, NSH3-V2, GKC, GKC[trunc]) were generated by PCR amplification using rat β_{2a}/pGW1 (Perez-Reyes et al., 1992) as template, followed by subcloning into pcDNA4.1 (Invitrogen) using BamHI and EcoRI sites. The deletion mutant GKC[ΔPYDVV] was generated by overlap extension PCR, followed by subcloning into pcDNA4.1 using BamHI and EcoRI sites. To generate XFP-tagged channel subunit fragments, full-length cyan fluorescent protein (CFP) and yellow fluorescent protein (YFP) (minus the stop codon) were amplified by PCR and cloned into pcDNA4.1 using KpnI and BamHI sites. The various channel fragments were then PCR amplified and cloned in-frame to the 3′ end of the appropriate XFP using BamHI and EcoRI sites. All PCR constructs were verified by sequencing.

Cell Culture and Transfection
For electrophysiology experiments, low-passage number HEK 293 cells plated on coverslips in 10-cm tissue culture dishes were transiently transfected with 8 μg α_{1C}-GFP, 8 μg each of the appropriate split-domain $Ca_V\beta$ fragment, and 3 μg T-antigen, using calcium-phosphate precipitation. To permit unambiguous identification of functional effects specific to the split-domain $Ca_V\beta_{2a}$ fragments, $\alpha_2\delta$ was omitted from transfections. For FRET experiments, HEK 293 cells were plated in culture dishes with No. 0 glass coverslip bottoms (MaTek) and transiently transfected with 0.5–3 μg XFP-tagged proteins using Fugene (Roche).

Electrophysiology
Whole-cell recordings were performed at room temperature 2–3 d after transfection using an EPC8 or EPC10 patch-clamp amplifier (HEKA Electronics) controlled by Pulse software (HEKA Electronics). Micropipettes were fashioned from 1.5-mm thin-wall glass with filament (WPI Instruments); series resistance was typically 2–4 MΩ and compensated 50–70%. A standard *I–V* protocol with 20-ms step depolarization (-40 to $+120$ mV) was used to evoke currents from a -100-mV holding potential. Tail currents were measured at -50-mV repolarization potential. Currents were sampled at 25 kHz and filtered at 10 kHz. Leak and capacitive transients were subtracted by P/8 protocol. External solution contained (in mM) 140 TEA-MeSO$_3$, 10 HEPES, 5 BaCl$_2$ (pH 7.3). Internal solution contained (in mM) 135 Cs-MeSO$_3$, 5 CsCl, 5 EGTA, 1 MgCl$_2$, 4 MgATP, 10 HEPES (pH 7.3). Recordings were analyzed off-line using PulseFit software (HEKA Electronics) and Ms Excel. *I-V* relations for each cell were fit to the following equation:

$$I = G(V - V_{rev})\frac{1}{1 + \exp\left(\frac{V_{1/2} - V}{k}\right)}, \qquad (1)$$

where I is the whole-cell current density (pA/pF), G is the specific conductance (pA pF^{-1} mV^{-1}), V_{rev} is the reversal potential

(mV), $V_{1/2}$ is the voltage of half-maximal activation (mV), and k is a slope factor (mV).

Normalized tail-activation data were fit to a double-Boltzmann function of the form

$$\frac{G}{G_{100}} = \frac{F_{low}}{1 + \exp\left(\frac{V_{1/2,low} - V}{k_{low}}\right)} + \frac{(1 - F_{low})}{1 + \exp\left(\frac{V_{1/2,high} - V}{k_{high}}\right)}, \quad (2)$$

where G is the tail current amplitude, G_{100} is the tail current amplitude elicited by a 100-mV test-pulse depolarization, F_{low} is the fraction of the low-threshold component, V is the test-pulse potential, $V_{1/2,low}$ and $V_{1/2,high}$, and k_{low} and k_{high} are the half-activation potentials and slope factors for the low- and high-threshold components, respectively.

FRET Measurements

Detection of protein interactions in live HEK 293 cells was accomplished using the three-cube FRET algorithm (Erickson et al., 2001, 2003). Transfected cells were washed with Tyrode solution and mounted on an inverted Nikon TE300 Eclipse microscope equipped for epifluorescence. A 150-W Xenon arc lamp served as excitation light source, and was gated by a computer-controlled shutter. Epifluorescence emission signals from individual cells were measured with a photomultiplier tube, integrated and filtered (10 kHz) by a fluorometer, and digitized. Autofluorescence and background levels were assessed from averages of individual untransfected cells and subtracted from experimental values for each cube. For each cell, measurements were taken with the following three-cube FRET filter cubes (excitation, dichroic, emission): CFP (440, 455, 480), YFP (500, 525, 530), and FRET (440, 455, 535). FRET ratio (*FR*) was calculated as

$$FR = \frac{[S_{FRET}(DA) - R_{D1} \bullet S_{CFP}(DA)]}{R_{A1} \bullet [S_{YFP}(DA) - R_{D2} \bullet S_{CFP}(DA)]}, \quad (3)$$

where S_{CUBE}(SPECIMEN) represents an intensity measurement, CUBE represents the filter cube, and SPECIMEN denotes whether the cell is expressing donor alone (D; CFP), acceptor alone (A; YFP), or both (DA). R_{D1} and R_{A1} are constants determined from cells expressing only CFP- or YFP-tagged molecules, respectively. Effective FRET efficiency (E_{EFF}) was determined from

$$E_{EFF} = E \times A_b = (FR - 1)\frac{[\in_{YFP}(440)]}{[\in_{CFP}(440)]}, \quad (4)$$

where E is the intrinsic FRET efficiency when particular XFP-tagged molecules associate with each other, A_b is the fraction of YFP-tagged molecules bound by CFP-tagged molecules, and the bracketed term is the ratio of the YFP and CFP molar extinction coefficients scaled for the FRET cube excitation filter.

Confocal Imaging

XFP-tagged fusion proteins were transiently transfected into HEK 293 cells cultured in MaTek tissue culture dishes. Confocal images were acquired 48 h post-transfection using an Olympus Fluoview laser scanning confocal microscope.

Statistics

Experimental parameters for various constructs were compared with those obtained with NSH3+GKC, and statistically significant differences (defined as P < 0.05) determined by the Student's *t* test. Linear regression was conducted using Excel with intercept set to zero. Multiple-regression analysis was performed in MS Excel to determine significant difference in fitted slopes. For *ON*-
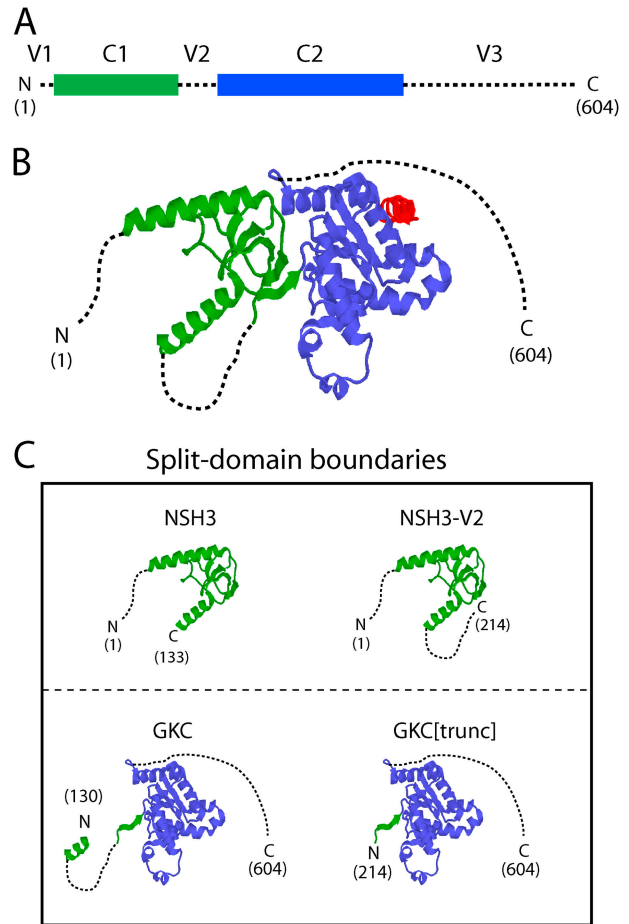

Figure 1. Ca$_V$β structure and split-domain boundaries. (A) Modular domain structure for Ca$_V$β$_{2a}$ based on primary sequence homology with other Ca$_V$β isoforms. Three variable regions (V1, V2, V3; dotted lines) are separated by two conserved domains (C1 and C2). (B) Crystal structures of the conserved core of Ca$_V$β subunits identify distinct SH3 (green) and GK (blue) domains in the two conserved domains. Variable regions are drawn in (dotted lines), but were not resolved in the crystal structures. The AID peptide (red) interacts exclusively with the GK domain. (C) Schematic displaying boundaries of split-domain Ca$_V$β$_{2a}$ constructs.

gating charge measurements, currents were leak subtracted using smooth curves fitted to leak pulses in IgorPro and analyzed in PulseFit. Data are mean ± SEM.

RESULTS

Location of Split Site in Split-domain Ca$_V$β$_{2a}$ Proteins Is an Important Determinant of Functional Channel Reconstitution

Ca$_V$βs contain SH3 and GK motifs in two conserved domains (Fig. 1, A and B). Recently, using a split-domain approach, we found that Ca$_V$β fragments containing either the SH3 (NSH3) or GK (GKC) domains (Fig. 1 C) could reconstitute wild-type Ca$_V$β functions only when both fragments were coexpressed with recombinant α$_{1C}$ (Takahashi et al., 2004). Fig. 2 A shows robust
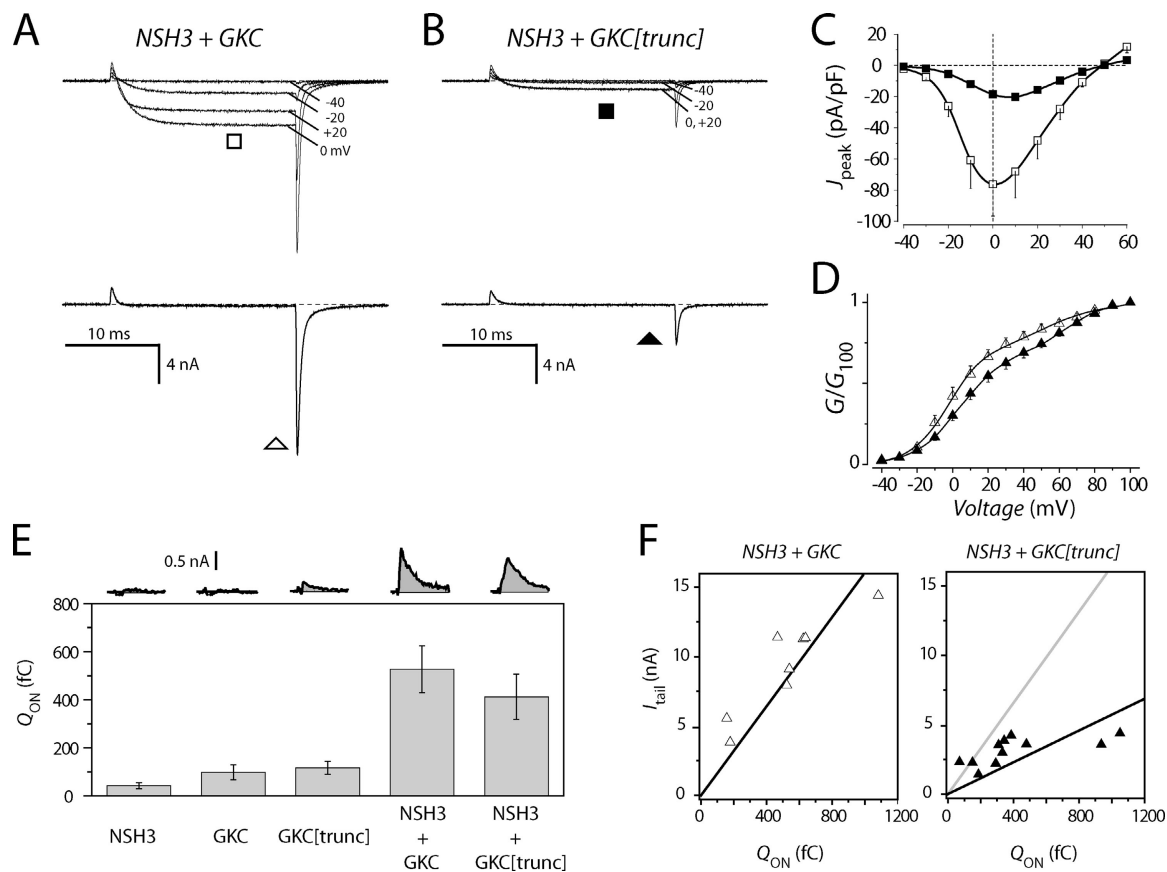
Figure 2. Distinctive channel modulation by split-domain $Ca_V\beta$ fragments differing in the split site. (A, top) Exemplar whole-cell Ba^{2+} currents evoked by a 25-ms test pulse to the indicated potentials from a HEK 293 cell transfected with α_{1C}/NSH3/GKC. Holding potential was -90 mV. (A, bottom) Exemplar current from the same cell evoked with a $+50$-mV test pulse shows good isolation of the ON gating current. Tail current was measured at a -50-mV repolarization potential. (B) Exemplar currents from a cell transfected with α_{1C}/NSH3/GKC[trunc]. Same format as A. (C) Population peak current versus voltage (J–V) relationship for recombinant L-type channels reconstituted with either NSH3+GKC ($\square$, $n = 9$ for each data point) or NSH3+GKC[trunc] ($\blacksquare$, $n = 11$ for each data point). (D) Normalized tail G–V relationships for channels reconstituted with NSH3+GKC ($\triangle$) or NSH3+GKC[trunc] ($\blacktriangle$). Smooth curves through the data are double-Boltzmann fits with the following parameters: for NSH3+GKC ($F_{low} = 0.72$, $V_{1/2,low} = -2.8$ mV, $V_{1/2,high} = 56.1$ mV, $k_{low} = 10.5$ mV, $k_{high} = 15.1$ mV), for NSH3+GKC[trunc] ($F_{low} = 0.69$, $V_{1/2,low} = 3.8$ mV, $V_{1/2,high} = 64.6$ mV, $k_{low} = 12.5$ mV, $k_{high} = 11.0$ mV). (E, top) Exemplar gating currents isolated at the reversal potential. (E, bottom) Q_{ON} measurements, $n = 6$–11 cells for each construct. (F, left) Scatter plot of tail current amplitude (I_{tail}) versus Q_{ON}, and regression line (slope = 16.3 pA/fC; R^2 = 0.95) for channels reconstituted with NSH3+GKC ($\triangle$). (F, right) I_{tail}–Q_{ON} scatter plot and regression line (black trace, slope = 5.7 pA/fC; R^2 = 0.79) for NSH3+GKC[trunc]-reconstituted channels. Regression line for NSH3+GKC channels is reproduced (gray) to facilitate direct visual comparison.

whole-cell currents from channels reconstituted with α_{1C}/NSH3/GKC that confirms the previous results. Moreover, we and others found that NSH3 and GKC (or similar split-domain proteins) can interact in trans (Opatowsky et al., 2003; McGee et al., 2004; Takahashi et al., 2004), raising the question of whether and how the $Ca_V\beta$ SH3–GK domain interaction is important for channel modulation (Takahashi et al., 2004). The most direct way to address this issue would be to selectively interfere with the $Ca_V\beta$ SH3–GK interaction while leaving the GK–AID interaction unchanged.

To explore the feasibility of this approach we initially truncated 84 residues from the amino terminus of GKC, generating GKC[trunc] (Fig. 1 C). The rationale

for this strategy stemmed from information provided by the $Ca_V\beta$ crystal structures showing that the AID–GK interaction surface is spatially removed from the SH3–GK interface (Fig. 1 B) (Chen et al., 2004; Opatowsky et al., 2004; Van Petegem et al., 2004). Before probing the actual effect of the 84-residue deletion on the status of the $Ca_V\beta$ SH3–GK interaction, we first determined whether channels reconstituted with NSH3+GKC[trunc] exhibited any gross functional distinctions compared with those formed with NSH3+GKC. Interestingly, whole-cell currents from NSH3+GKC[trunc]-reconstituted L-type channels were significantly smaller in amplitude (Fig. 2 B) compared with their NSH3+GKC-reconstituted counterparts (Fig. 2 A). The deficit

Effects of Distinct Split-domain Ca$_V$β Configurations on Gating Properties of Recombinant L-type Ca^{2+} Channels

Transfected constructs	G	$V_{1/2}$	k	n
	$pApF^{-1}mV^{-1}$	mV	mV	
NSH3+GKC	1.73 ± 0.41	−13.9 ± 1.4	5.64 ± 0.29	9
NSH3-V2+GKC	1.83 ± 0.52	−11.6 ± 1.3	6.49 ± 0.34	6
NSH3+GKC[trunc]	0.52 ± 0.06[a]	−7.8 ± 1.4[a]	6.91 ± 0.13[a]	11
NSH3-V2+GKC[trunc]	0.39 ± 0.07[a]	−7.5 ± 1.5[a]	7.88 ± 0.22[a]	6
GKC[ΔPYDVV]	0.09 ± 0.01[a]	−6.2 ± 1.1[a]	6.98 ± 0.43[a]	5
NSH3+GKC[ΔPYDVV]	0.09 ± 0.02[a]	−6.6 ± 2.1[a]	8.23 ± 0.51[a]	5

[a]P < 0.05, compared to NSH3+GKC-reconstituted channels.

in current amplitude extended across the entire range of test pulse voltages, with no change in reversal potential between the two channel types as indicated by population current density (J_{peak}) versus voltage (J–V) plots (Fig. 2 C). Beyond the deficits in whole-cell current amplitude, normalized tail activation plots demonstrated that NSH3+GKC[trunc] channels displayed a right-shifted voltage dependence of channel activation compared with channels reconstituted with NSH3+GKC (Fig. 2 D), revealing an inability to recapitulate this functional hallmark (i.e., a hyperpolarizing shift in channel activation) of Ca$_V$β regulation. Overall, NSH3+GKC[trunc] channels displayed an over three-fold decrease in peak current density, a 6-mV rightward shift in $V_{1/2}$ of activation, and a significant decrease in the steepness of voltage dependence of channel activation, compared with channels reconstituted with NSH3+GKC (Table I).

What molecular mechanisms underpinned the functional differences between channels reconstituted with NSH3+GKC and NSH3+GKC[trunc], respectively? Mechanistic insights were gained from considering that whole-cell current (I) is related to microscopic channel properties by the relation $I = N \times i \times P_o$, where N is the number of channels at the membrane, and i is the unitary current amplitude. Ca$_V$βs do not affect i (Hullin et al., 2003), as might be expected from cytosolic auxiliary proteins that do not alter the permeation pathway of the channel. Hence, differential alterations of N and P_o likely underlie the distinctions in how NSH3+GKC and NSH3+GKC[trunc] reconstitute whole-cell currents. Fortunately, further analyses of our whole-cell experimental records permit useful comparative evaluation of the relative effects of NSH3+GKC and NSH3+GKC[trunc] on N and P_o. The time integral of the ON gating current isolated at the reversal potential (Fig. 2, A and B, bottom traces) yields the ON gating charge (Q_{ON}), which provides a convenient index of N (Q_{ON} = Nq; Wei et al., 1994; Takahashi et al., 2004). Exemplar traces (Fig. 2, A and B, bottom traces) hinted that despite the clearly divergent whole-cell current amplitude

(as reported by tail current size), gating-current size was quite similar between NSH3+GKC and NSH3+GKC[trunc] channels. This impression was confirmed in the population data (Fig. 2 E). As previously reported (Takahashi et al., 2004), neither NSH3 nor GKC alone could efficiently transport α$_{1C}$ to the membrane, whereas NSH3+GKC restored trafficking to wild-type Ca$_V$β$_{2a}$ levels, as gauged by Q_{ON} measurements. As expected, GKC[trunc] alone was also unable to rescue channel trafficking. The surprising new result was that NSH3+GKC[trunc] also restored N (Fig. 2 E), belying its modest effects on whole-cell current amplitude (Fig. 2 C). This discrepancy suggested that NSH3+GKC and NSH3+GKC[trunc] might have rather divergent effects on channel P_o. We sought direct confirmation of this difference using a slope analysis method (Fig. 2 F). Here, the regression line slope of a plot of tail current amplitude obtained at the reversal potential (typically +50 mV; I_{tail}) versus Q_{ON} provides a convenient metric for relative P_o (Wei et al., 1994; Takahashi et al., 2004). By this analysis, channels reconstituted with NSH3+GKC[trunc] displayed a lower P_o, as indicated by a significantly shallower slope compared with NSH3+GKC (Fig. 2 F; slope = 16.3 ± 3.2 pA/fC [95% CI] for NSH3+GKC, △; slope = 5.7 ± 2.1 pA/fC for NSH3+GKC[trunc], ▲; P < 0.001 by multiple regression). Therefore, the deficit in whole-cell current amplitude obtained with NSH3+GKC[trunc] is due specifically to an inability of this split-domain pair to reconstitute the increased-P_o function of Ca$_V$β.

Overall, the functional differences between NSH3+GKC and NSH3+GKC[trunc]-reconstituted channels could be consistent with one of two competing hypotheses. The first stems from the fact that NSH3+GKC[trunc] lacks 81 amino acids (spanning the latter region of the first conserved domain [C1] and the entire alternatively spliced second variable domain [V2]) compared with either wild-type β$_{2a}$ or NSH3+GKC (Fig. 1). Hence, the lack of an effect of NSH3+GKC[trunc] on activation gating and P_o could simply reflect an essential role of this absent region in transducing these gating properties. Alternatively, the functional distinctions between NSH3+GKC and NSH3+GKC[trunc] could be directly due to variations in the Ca$_V$β SH3–GK domain interaction between the two split-domain configurations. To discriminate between these two hypotheses, we generated a new SH3-containing split-domain Ca$_V$β$_{2a}$ variant (termed NSH3-V2) that included the first three domains of β$_{2a}$ (Fig. 1 C). Accordingly, NSH3-V2+GKC[trunc] now spanned all of the Ca$_V$β$_{2a}$ sequence, thereby addressing ambiguities arising from the loss of 81 amino acids in NSH3+GKC[trunc].

Functionally, electrophysiological data obtained from channels reconstituted with NSH3-V2+GKC[trunc]
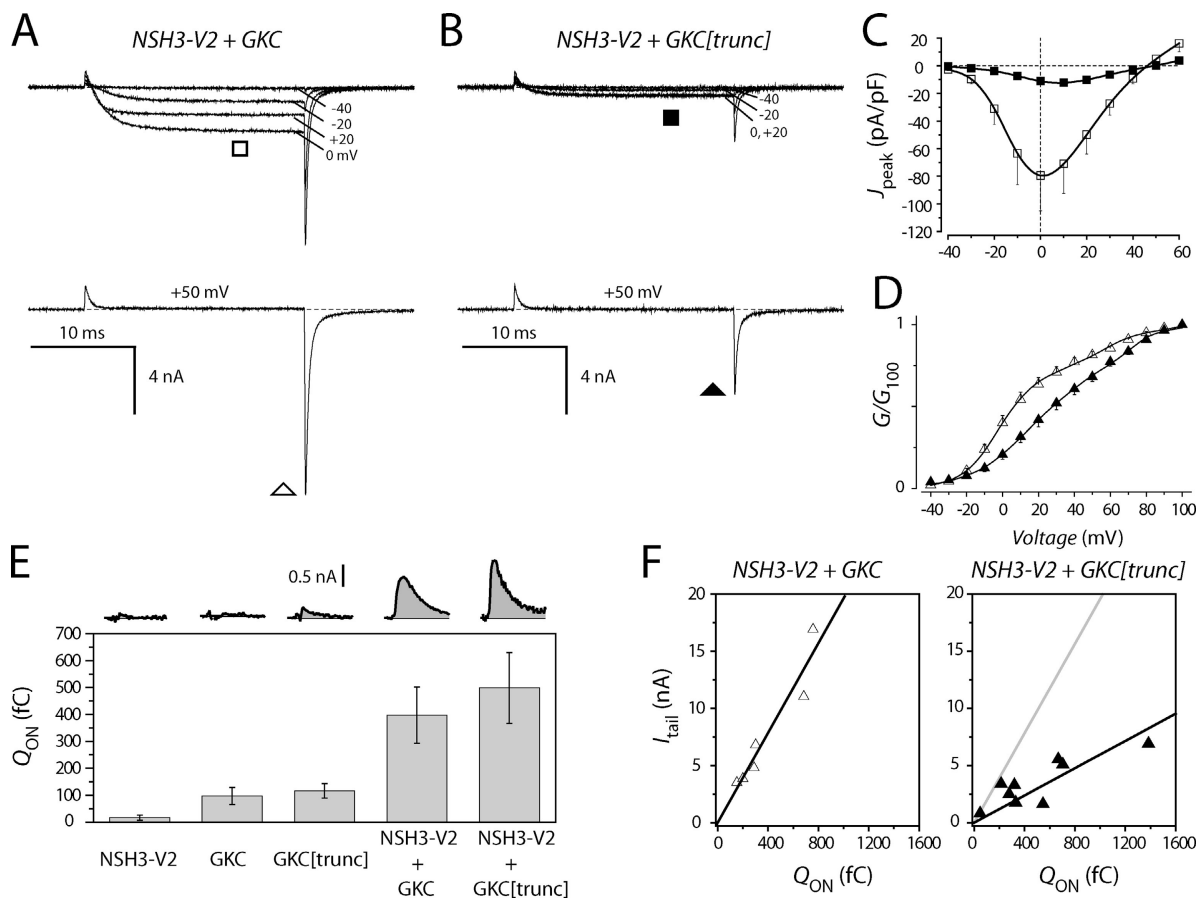
Figure 3. The split site, and not the loss of 81 residues, is responsible for functional deficiencies of channels reconstituted with GKC[trunc]. (A–F) Exemplar currents and population plots for channels reconstituted with NSH3-V2+GKC and NSH3-V2+GKC[trunc], respectively. Format identical to Fig. 2 legend. Smooth fits in D have the following parameters: for NSH3-V2+GKC (F_{low} = 0.70, $V_{1/2,low}$ = −2.6 mV, $V_{1/2,high}$ = 56.0 mV, k_{low} = 10.6 mV, k_{high} = 14.5 mV), for NSH3-V2+GKC[trunc] (F_{low} = 0.75, $V_{1/2,low}$ = 16.1 mV, $V_{1/2,high}$ = 70.2 mV, k_{low} = 17.0 mV, k_{high} = 9.6 mV). For regression lines in F, slope = 19.6 pA/fC, R^2 = 0.98 for NSH3-V2+GKC; slope = 5.96 pA/fC, R^2 = 0.89 for NSH3-V2+GKC[trunc] channels.

(Fig. 3) were essentially identical to that obtained with NSH3+GKC[trunc] (Table I). NSH3-V2+GKC[trunc] was unable to recover the bulk of whole-cell current amplitude (Fig. 3, A–C), did not recapitulate the hyperpolarizing shift in channel activation gating (Fig. 3 D), and did not restore the increased-P_o property (Fig. 3 F, ▲; slope = 5.96 ± 1.69 pA/fC; P < 0.001 compared with NSH3-V2+GKC, △). However, NSH3-V2+GKC[trunc] fully restored the channel trafficking function (Fig. 3 E). By contrast, NSH3-V2+GKC recovered wild-type whole-cell current amplitude (Fig. 3, A–C) by reconstituting both the trafficking (Fig. 3 E) and enhanced-P_o functions (Fig. 3 F, △), and also recapitulated the hyperpolarizing shift in the voltage dependence of channel activation (Fig. 3 D; Table I). Together, these results affirmed the unexpected result that a simple difference in the cut site of split-domain $Ca_V\beta$ constructs can uncouple the trafficking and gating-modulation functions. Moreover, these results ruled out the explanation that NSH3+GKC[trunc] did

not recover the gating-modulation functions simply because of the mere absence of an 81–amino acid central segment of $Ca_V\beta_{2a}$. This raised the idea that functional disparities between channels reconstituted with NSH3 (or NSH3-V2) and GKC or GKC[trunc], respectively, might be due to differences in the status of the $Ca_V\beta$ SH3–GK domain interaction. Accordingly, we next sought direct evidence for potential variations in the way in which GKC and GKC[trunc] interacted with NSH3.

Probing $Ca_V\beta$ Domain Interactions by Live-cell FRET Reveals Subtle Distinctions between GKC and GKC[trunc] in their Binding to NSH3

We adopted the optical FRET two-hybrid approach (Erickson et al., 2003) to probe for interactions between split-domain $Ca_V\beta$ constructs (Fig. 4). This approach offered the advantage of reporting on the status of split-domain $Ca_V\beta$ SH3–GK interactions in the relevant setting of live HEK 293 cells, permitting a di-

rect correlation of binding properties and functional electrophysiological experiments. Coding sequences for enhanced CFP and enhanced YFP were fused upstream of those for NSH3 and the two GK domain constructs, respectively. Confocal images of live cells show the subcellular localization of the distinct XFP-tagged proteins upon their cotransfection in HEK 293 cells (Fig. 4 A). CFP-NSH3 localized uniformly throughout the cell, with similar fluorescent intensity in the cytoplasm and the nucleus (Fig. 4 A, left). This distribution presumably reflects the fact that the relatively small size of CFP-NSH3 permits passive diffusion into the nucleus. By contrast, both YFP-GKC and YFP-GKC[trunc] were uniformly present in the cytosol, and excluded from the nucleus (Fig. 4 A, right). Importantly, the mean fluorescence intensities for YFP-GKC and YFP-GKC-[trunc] were not significantly different (Fig. 4 B; P = 0.07), indicating no dramatic differences in expression levels between these two proteins. This finding rules out the trivial possibility that the observed functional divergence between GKC and GKC[trunc] (Figs. 2 and 3) could be due to large differences in expression levels or protein stability between the two.

To evaluate interactions between split-domain $Ca_V\beta$ SH3 and GK proteins, we used a three-cube FRET algorithm (Erickson et al., 2001). This method enables calculation of FRET efficiencies despite excitation cross talk between CFP and YFP, and inescapable variability in the ratio of CFP- and YFP-tagged molecules in a given cell (Erickson et al., 2001, 2003). The three-cube FRET method permits sensitive detection of protein interactions as measured by the FRET ratio (FR; the fold increase in YFP fluorescence due to FRET), or effective FRET efficiency (E_{EFF}): $FR = 1$ indicates no FRET, whereas $FR > 1$ indicates detection of FRET, and hence, an interaction between CFP- and YFP-tagged proteins. Application of this analysis to cells cotransfected with CFP-NSH3 and YFP-GKC yielded $FR = 2.8 \pm 0.1$ ($E_{EFF} = 10.2 \pm 0.4\%$; $n = 25$), indicating an interaction between these two proteins in HEK 293 cells (Fig. 4 C). This was reassuring given previous results that identical or similar split-domain $Ca_V\beta$ fragments interact, as determined by in vitro protein binding and yeast two-hybrid assays (Opatowsky et al., 2003; McGee et al., 2004; Takahashi et al., 2004). Control experiments featuring cells expressing CFP-NSH3+YFP, CFP+YFP-GKC, and CFP+YFP-GKC[trunc] displayed uniformly low FR (≤ 1.2) and E_{EFF} ($\leq 1\%$) values (Fig. 4 C), demonstrating the specificity of the assay. The important new result was that cells cotransfected with CFP-NSH3 and YFP-GKC[trunc] also exhibited robust FRET ($FR = 3.7 \pm 0.1$; $E_{EFF} = 15.5 \pm 0.4\%$, $n = 26$), indicating an interaction between these two $Ca_V\beta_{2a}$ fragments. This result showed that the deficiency of
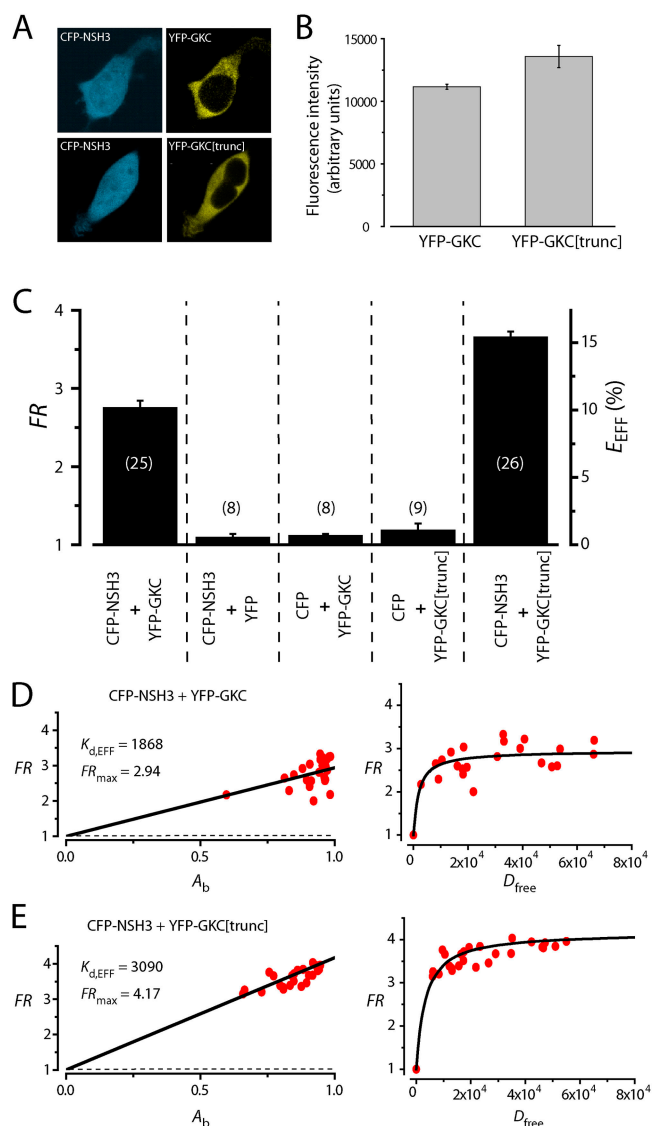

Figure 4. Probing $Ca_V\beta$ split-domain interactions by three-cube FRET. (A) Confocal images of a HEK 293 cell coexpressing CFP-NSH3 and YFP-GKC (top), or CFP-NSH3 and YFP-GKC[trunc] (bottom). (B) Mean fluorescent intensities for YFP-GKC ($n = 25$) and YFP-GKC[trunc] ($n = 26$) molecules measured in transfected HEK 293 cells. (C) Population FR and E_{EFF} measurements. (D and E) Fits of FR scatter plots for CFP-NSH3+YFP-GKC and CFP-NSH3+YFP-GKC[trunc] to a 1:1 binding model.

NSH3+GKC[trunc] in rescuing whole-cell current and increased-P_o was not due to an outright ablation of the $Ca_V\beta$ SH3–GK domain interaction.

We next sought to determine whether there were quantitative distinctions between the binding of GKC and GKC[trunc] to NSH3 that might account for the observed functional differences. To accomplish this we took advantage of the capability of the three-cube FRET method to yield an estimate of the in situ dissociation constant governing interaction between XFP-tagged molecules (Erickson et al., 2003). The approach
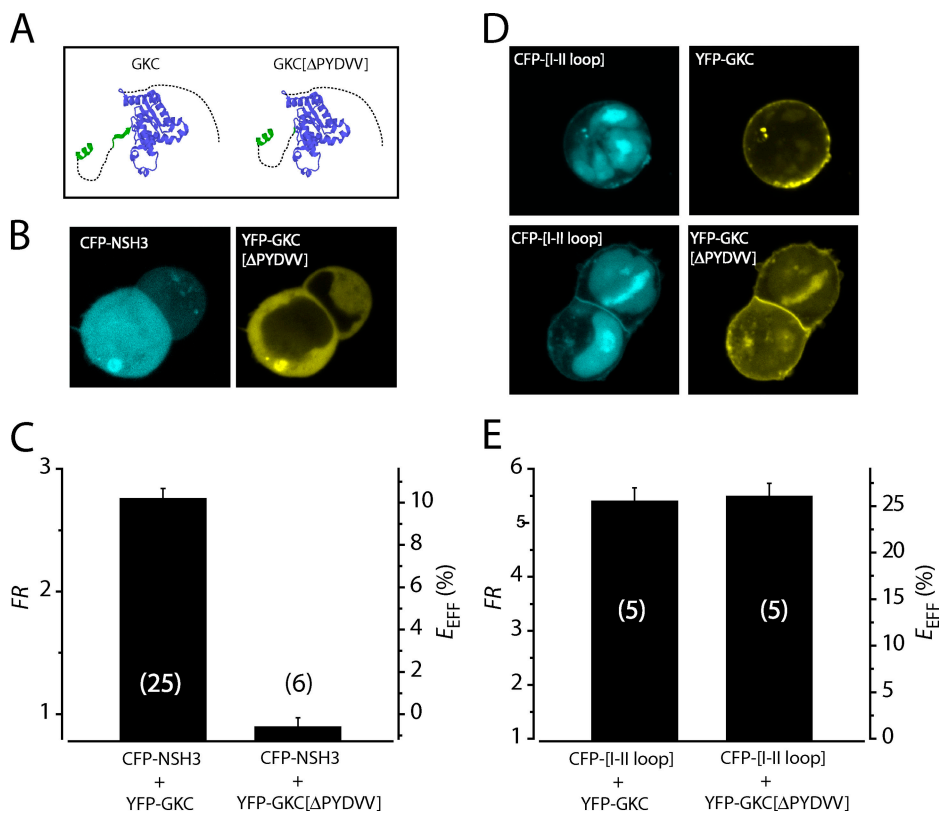
Figure 5. Deletion of a SH3 β5 strand selectively ablates the $Ca_V\beta$ SH3–GK interaction. (A) Cartoon comparing structures of GKC and GKC[ΔPYDVV]. (B) Confocal slices showing subcellular localization of CFP-NSH3 and YFP-GKC[ΔPYDVV]. (C) Population FR and E_{EFF} measurements for $Ca_V\beta$ SH3/GK domain interactions. (D) Confocal slices showing subcellular localization of CFP-α_{1C}[I-II loop] and distinct YFP-tagged $Ca_V\beta$ GK domains. (E) Population FR and E_{EFF} measurements for α_{1C}[I-II loop]/GK domain interactions.

exploits the inevitable variability in the expression ratios of CFP- and YFP-tagged molecules in distinct transfected cells. FR reflects both the intrinsic FRET coupling between interacting pairs of molecules and the fraction of YFP-tagged molecules bound by a CFP-tagged molecule (A_b). Fitting FRET measurements from different cells to a 1:1 binding model yields two parameters, the relative dissociation constant $K_{d,EFF}$ (which is proportional to the actual K_d) and the maximal FR (FR_{max}) attained when A_b is unity (Erickson et al., 2003). Alternatively, FR can be plotted versus D_{free}, a measure of the relative concentration of tagged donor molecules. Application of this analysis to CFP-NSH3+YFP-GKC (Fig. 4 D) and CFP-NSH3+YFP-GKC[trunc] (Fig. 4 E) yielded $K_{d,EFF}$ values of 1868 and 3090, respectively, indicating a maintained high-affinity interaction in both split-domain SH3–GK pairs. By contrast, FR_{max} was significantly different in the two cases (2.94 for CFP-NSH3+YFP-GKC and 4.17 for CFP-NSH3+YFP-GKC[trunc]), suggesting distinctions in the relative geometric orientations of the SH3 and GK domains in the two split-domain configurations. Overall, these results show that GKC and GKC[trunc] display only subtle distinctions in how they bind NSH3. Nevertheless, it appears that even such small differences in the arrangement of the $Ca_V\beta$ SH3–GK interaction can produce disproportionately large functional effects on Ca^{2+} channel behavior.

Deletion of a Five-residue β5 Strand Selectively Ablates the $Ca_V\beta$ SH3–GK Domain Interaction while Preserving the GK–AID Association

To gain insight into whether the SH3 and GK domains could act independently to reconstitute any aspect of $Ca_V\beta$ function, it was necessary to selectively ablate the $Ca_V\beta$ SH3–GK interaction, while preserving the GK–AID interaction. Our previous work hinted that a point mutation in the $Ca_V\beta_{2a}$ GK domain (P234R) effectively disrupted the intramolecular SH3–GK interaction (Takahashi et al., 2004). A similar result was obtained with a truncation that eliminated five carboxy-terminal residues from the $Ca_V\beta$ GK domain (McGee et al., 2004). However, neither of these mutations is suitable to determine the independence of the $Ca_V\beta$ SH3 and GK domains because the disruption of the SH3–GK interaction in both cases is not selective; both mutants are expected to disrupt the global GK fold, and thus also ablate the GK–AID interaction (De Waard et al., 1994; Chen et al., 2004; Opatowsky et al., 2004; Van Petegem et al., 2004). Likewise, a point mutation in the $Ca_V\beta_{2a}$ SH3 domain (L93P) also disrupted the $Ca_V\beta$ SH3–GK interaction (McGee et al., 2004; Takahashi et al., 2004). However, the effect of this mutation on the ternary structure of the SH3 domain is unknown. It is also unknown whether the L93P mutation abolishes potentially relevant interactions of $Ca_V\beta$ SH3 with the α_1 subunit. Hence, to date, there is a lack of $Ca_V\beta$ mutations
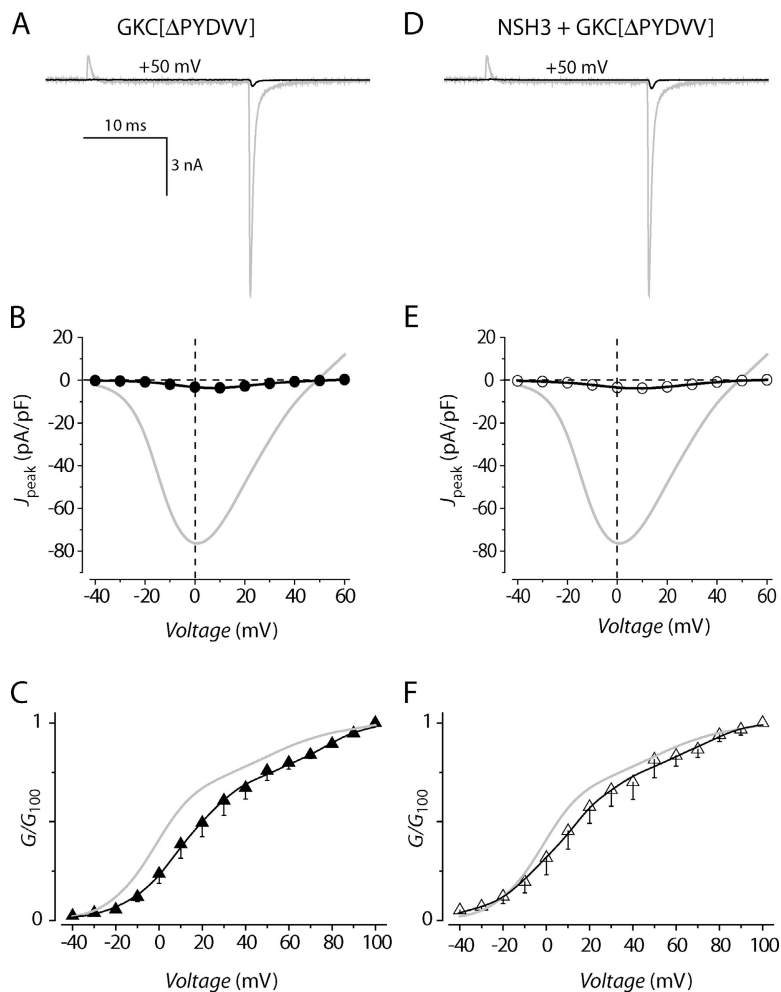
Figure 6. Ablation of the SH3–GK association abolishes synergistic functional interactions between $Ca_V\beta$ SH3 and GK domains. (A) Exemplar current trace from a recombinant L-type channel reconstituted with GKC[ΔPYDVV] alone was evoked at a test potential of +50 mV. Tail current was measured at a −50-mV repolarization potential. Exemplar current from a channel reconstituted with NSH3+GKC is reproduced (gray trace) to facilitate direct visual comparison. (B) Population J–V relationship for GKC[ΔPYDVV]-reconstituted channels. Data for NSH3+GKC is reproduced (gray trace) for comparison. (C) Normalized tail G–V relationship for GKC[ΔPYDVV]-reconstituted channels (▲). Double-Boltzmann fit to the data (smooth curve) had the following parameters: $F_{low} = 0.75$, $V_{1/2,low} = 10.9$ mV, $V_{1/2,high} = 74.3$ mV, $k_{low} = 13.4$ mV, $k_{high} = 11.0$ mV. Corresponding fit for NSH3+GKC is reproduced (gray trace) for comparison. (D–F) Data for channels reconstituted with NSH3+GKC[ΔPYDVV]. Identical format as A–C. Double-Boltzmann fit in F had the following parameters: $F_{low} = 0.82$, $V_{1/2,low} = 7.4$ mV, $V_{1/2,high} = 72.9$ mV, $k_{low} = 15.9$ mV, $k_{high} = 9.6$ mV.

that unambiguously permit assessment of whether the SH3 and GK domains can act independently to reconstitute $Ca_V\beta$ functions.

To address this deficiency, we focused attention on a five-residue β5 strand (that occurs immediately after the variable V2 domain and is formally a part of the SH3 domain) that the crystal structures suggested is crucial for keeping the two domains together by interacting with residues in both the SH3 and GK domains (Opatowsky et al., 2003; Chen et al., 2004; Van Petegem et al., 2004). We hypothesized that deleting the β5 strand would selectively ablate the $Ca_V\beta$ SH3–GK interaction. To test this, we deleted the β5 strand from GKC, generating GKC[ΔPYDVV] (Fig. 5 A). YFP-GKC[ΔPYDVV] was diffusely localized throughout the cytosol and excluded from the nucleus (Fig. 5 B, right), similar to the subcellular localization of YFP-GKC (Fig. 4 A). Three-cube FRET experiments revealed that YFP-GKC[ΔPYDVV] did not interact with CFP-NSH3 ($FR = 0.9 \pm 0.07$, $n = 6$) indicating a successful ablation of the SH3–GK interaction (Fig. 5 C), and affirming the critical role of the β5 strand in keeping the two domains together.

It was important to our goals to ensure that deleting the β5 strand did not cause a global disruption of the GK domain. To address this, we probed for the ability of YFP-GKC and YFP-GKC[ΔPYDVV] to interact with CFP-α_{1C}[I-II loop] by FRET. CFP-α_{1C}[I-II loop] had an unexpected, but fortuitous subcellular localization (Fig. 5 D, left). The protein was present in the nucleus, likely reflecting its small size permitting passive diffusion across the nuclear membrane. More surprising was its localization to the plasma membrane, with little representation in the cytosol (Fig. 5 D, left). YFP-GKC, when cotransfected with CFP-α_{1C}[I-II loop] no longer localized diffusely in the cytosol, as observed when it was cotransfected with CFP-NSH3 (Fig. 4 A), but instead was highly enriched at the plasma membrane (Fig. 5 D, top right). This relocation provided an immediate visual affirmation that YFP-GKC was interacting with CFP-α_{1C}[I-II loop], a fact that was confirmed by a robust FRET signal ($FR = 5.4 \pm 0.2$; $E_{EFF} = 25.6 \pm 1.4\%$, $n = 5$) between the two proteins. Importantly, YFP-GKC[ΔPYDVV] behaved similarly to YFP-GKC with respect to sub-cellular relocation (Fig. 5 D, bottom right) and FRET signal ($FR = 5.5 \pm 0.2$; $E_{EFF} = 26.1 \pm$

1.4%, $n = 5$) when cotransfected with CFP-α_{1C}[I-II loop]. Given the precise three-dimensional architecture of the α_1-binding pocket on Ca$_V\beta$s (Chen et al., 2004; Opatowsky et al., 2004; Van Petegem et al., 2004), these findings indicate that deleting the β5 strand does not disrupt the global folding of the GK domain. Therefore, the ΔPYDVV deletion mutation fulfills the crucial criteria of selectively ablating the Ca$_V\beta$ SH3–GK interaction while preserving the GK–AID association, enabling the first direct test of whether SH3 and GK domains could act independently to reconstitute aspects of Ca$_V\beta$ function.

Selective Ablation of the SH3–GK Interaction Abolishes the Synergism between Split-domain Ca$_V\beta$ SH3- and GK-containing Fragments

To determine the functional effects of ablating the Ca$_V\beta$ SH3–GK interaction we turned to whole-cell electrophysiological experiments. GKC[ΔPYDVV] expressed alone with α_{1C} was deficient in its ability to rescue whole-cell currents (Fig. 6, A and B; Table I) and to induce a hyperpolarizing shift in activation gating (Fig. 6 C; Table I), despite its demonstrated normal binding to the α_{1C}[I-II loop] (Fig. 5 E). These results confirm our previous finding that the GK domain is insufficient to reconstitute the bulk of Ca$_V\beta$ modulatory properties in HEK 293 cells (Takahashi et al., 2004). The new insight came with studying the effects of NSH3+GKC [ΔPYDVV] on Ca^{2+} channel currents. Channels reconstituted with NSH3+GKC[ΔPYDVV] behaved similarly to those obtained with GKC[ΔPYDVV] alone, with respect to whole-cell current amplitude (Fig. 6, D and E; Table I) and the voltage dependence of channel activation (Fig. 6 F; Table I). These results contrast sharply with the synergism observed between NSH3 and GKC (Takahashi et al., 2004), and revealed that the SH3–GK interaction is requisite for Ca$_V\beta$ modulation of channel trafficking and gating. Overall, these results are consistent with a co-dependent model for Ca$_V\beta$ SH3 and GK domains to modulate channel function.

NSH3 Can Interact Independently with the α_{1C} Subunit

The lack of effect of NSH3 on channel properties when cotransfected with GKC[ΔPYDVV] gave reason to wonder whether NSH3 could actually bind to α_{1C} independently of an interaction with a Ca$_V\beta$ GK domain. Previous in vitro studies have indicated that the Ca$_V\beta$ SH3 domain may interact weakly with the α_{1C} I-II loop (Maltez et al., 2005) or the carboxy tail (Gerhardstein et al., 2000), but an association with α_1 subunit in the context of living cells has not been demonstrated. To address this, we probed for an interaction between CFP-NSH3 and YFP-α_{1C} by FRET. We used an α_{1C} subunit that was truncated at the carboxy terminus (α_{1C}[1671]) to maximize the chances of observing
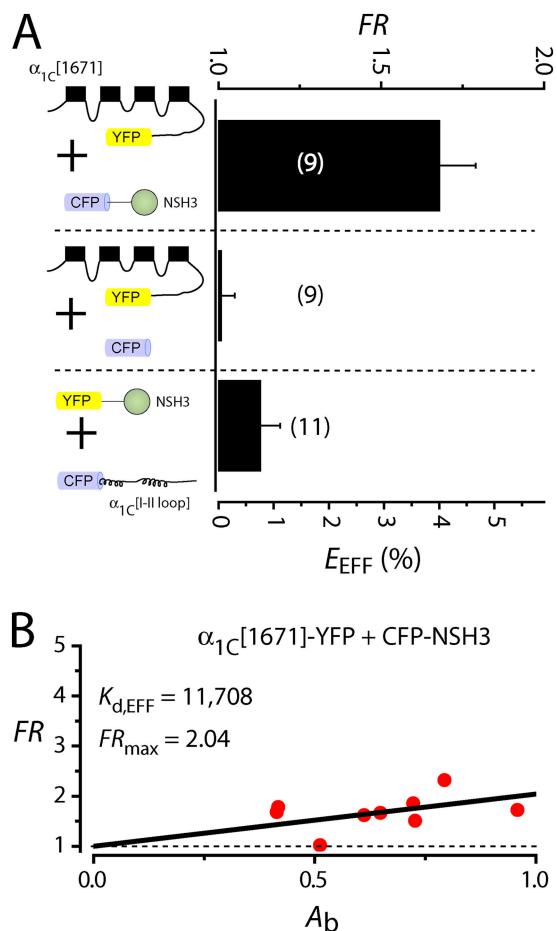

Figure 7. NSH3 can interact independently with α_{1C}. (A) Population FR and E_{EFF} measurements for α_{1C}-YFP+CFP-NSH3, α_{1C}-YFP+CFP, and YFP-NSH3+CFP-α_{1C}[I-II loop]. (B) Binding analyses on FR scatter plot for α_{1C}-YFP+CFP-NSH3.

FRET. Previous studies had shown that this truncated α_1 was still dependent on Ca$_V\beta$ for trafficking and gating modulation (Erickson et al., 2001). Compared with control cells expressing CFP+YFP-α_{1C}, test group cells coexpressing CFP-NSH3 and YFP-α_{1C} displayed a significantly elevated FRET ($FR = 1.68 \pm 0.11$, $n = 9$ for test-group cells; $FR = 1.01 \pm 0.04$, $n = 9$ for control cells; P < 0.001). Therefore, NSH3 is able to independently associate with α_{1C} in live HEK 293 cells. Furthermore, fits of the FRET data to a 1:1 binding model yielded a $K_{d,EFF} = 11{,}708$, indicating that the NSH3/α_{1C} interaction was of a significantly lower affinity than the NSH3/ GKC interaction. Moreover, this value is dramatically higher than one previously estimated for full-length Ca$_V\beta_{2a}$ binding to α_{1C} ($K_{d,EFF} = 43$) (Erickson et al., 2001). This is in agreement with the idea that the GK domain is primarily responsible for high-affinity binding of Ca$_V\beta$ to α_1 subunits, compared with the SH3 domain. To determine whether NSH3 interacted with α_{1C}

primarily via the cytoplasmic domain I-II loop (Maltez et al., 2005), we investigated an association between YFP-NSH3 and CFP-α_{1C}[I-II loop] by FRET. This experiment yielded a low *FR* value (Fig. 7 A, *FR* = 1.13 ± 0.06) that was not significantly different from the control case of YFP + CFP-NSH3 (Fig. 4 C, *FR* = 1.10 ± 0.04, P = 0.67). Hence the low-affinity interaction between NSH3 and the α_1-subunit I-II loop may be below the threshold detectable by the FRET assay. Together with the identified FRET interaction between YFP-α_{1C} and CFP-NSH3, the results suggest that NSH3 primarily binds to α_{1C} at a site that is different from the I-II loop.

Overall, the results indicate that the inability of NSH3 to influence channel properties when coexpressed with GKC[ΔPYDVV] is not because it cannot interact with α_{1C}. Instead, taken together, the results reveal the dominance of the SH3–GK interaction in dictating $Ca_V\beta$ modulation of multiple functional properties of high voltage–activated Ca^{2+} channels.

DISCUSSION

This study makes two main findings. (1) Although both the SH3 and GK domains are necessary to fully recapitulate $Ca_V\beta$ modulation of Ca^{2+} channels, they cannot act independently to reconstitute $Ca_V\beta$ function. (2) Subtle alterations in the inter-relationship of the SH3 and GK domains can uncouple the $Ca_V\beta$ trafficking and gating-modulation functions. The data have important implications for insights into the structure–function of the Ca^{2+} channel α_1–β interaction, and are also noteworthy for describing new mechanistic paradigms for an SH3–GK module that is widely conserved among MAGUK proteins. We discuss these ramifications of the work in relation to previous findings.

Ca^{2+} Channel Structure–Function Implications

It was previously believed that the second conserved domain of $Ca_V\beta$s, which constitutes a GK motif, predominantly encoded the channel regulation properties of $Ca_V\beta$s, via its high-affinity interaction with the AID (De Waard et al., 1994; Pragnell et al., 1994; Chen et al., 2004; Opatowsky et al., 2004; Van Petegem et al., 2004). However, recent functional studies pointed to an unexpectedly prominent role of the $Ca_V\beta$ SH3 domain in modulating both channel trafficking and gating (Opatowsky et al., 2003; Takahashi et al., 2004; Maltez et al., 2005). A new insight from the present work is that the $Ca_V\beta$ SH3 and GK domains do not act independent of each other to reconstitute function. This finding is at odds with a prevailing model that $Ca_V\beta$s promote channel trafficking by masking an ER retention signal in the α_1 subunit domain I-II linker (Bichet et al., 2000). Specifically, our results are inconsistent with the sufficiency of this mechanism because

binding to the I-II loop can occur without appreciable channel trafficking (as observed with GKC and GKC[trunc] alone; Fig. 2 E and Fig. 5 E). Moreover, our results are also inconsistent with the idea that the SH3 domain simply masks another ER retention signal elsewhere in the channel to synergistically promote channel trafficking. If that were the case, then the SH3 and GK domains would be expected to be able to reconstitute channel trafficking in an independent fashion. Instead, we found that NSH3 and GKC[ΔPYDVV] (which do not interact) could not reconstitute efficient α_{1C} trafficking to the membrane, even though both split-domain motifs were capable of engaging their respective binding sites on the α_{1C} subunit. The requirement for the $Ca_V\beta$ SH3–GK interaction to reconstitute the channel trafficking function could signify two things. First, it could serve to increase the effective local concentration of the SH3 domain so that it engages its relatively low-affinity binding site on α_1 (Maltez et al., 2005). This scenario appears somewhat unlikely since we demonstrate that freely expressed NSH3 is quite capable of interacting with α_{1C} by itself. Alternatively, the SH3–GK interaction could ensure that $Ca_V\beta$ binding to α_1 subunit occurs according to an induced fit model, effectively promoting an α_1 conformation favorable for channel trafficking to the membrane.

Another important finding was that the α_{1C} subunit was exquisitely attuned to the status of the $Ca_V\beta$ SH3–GK interaction; relatively subtle changes in the configuration of the $Ca_V\beta$ SH3–GK domain interaction selectively ablated gating-modulation (increased-P_o and hyperpolarizing shift in voltage dependence of activation gating) functions, whereas channel trafficking capabilities were preserved. Thus, trafficking and gating modulation are separable functions of $Ca_V\beta$ based on the arrangement of the SH3–GK interaction. Previous studies have also found that trafficking and gating modulation are independent functions of $Ca_V\beta$. In one study, the two processes could be separated based on different $Ca_V\beta$ concentration dependencies; low $Ca_V\beta$ concentrations selectively recapitulated channel trafficking, whereas higher amounts were needed to reconstitute gating modulation (Canti et al., 2001). A second study found that a mutation in the AID of α_{1C} (α_{1C}[Y467S]) disrupted the ability of $Ca_V\beta$ to traffick the channel, whereas gating modulation of whole-cell and single-channel currents was maintained (Gerster et al., 1999). Our findings raise the exciting possibility that the $Ca_V\beta$ SH3–GK interaction may be targeted by physiological and, possibly, pharmacological messengers as a means to modulate Ca^{2+} channel activity. In this regard, our development of a FRET-based method to monitor $Ca_V\beta$ SH3–GK interactions in live cells should hasten discovery in such new dimensions of Ca^{2+} channel research.

Comparisons to MAGUK SH3–GK Structure–Function

$Ca_V\beta$s and MAGUK family proteins share the common design principle of containing an SH3–GK structural module (Anderson, 1996; Funke et al., 2004). In addition, MAGUKS typically have one or more PDZ domains that are lacking in $Ca_V\beta$s. The crystal structure of the SH3–GK core from PSD-95 revealed an intramolecular SH3–GK interaction (McGee et al., 2001; Tavares et al., 2001), although the structural details differ somewhat from that observed with $Ca_V\beta$s (Chen et al., 2004; Opatowsky et al., 2004; Van Petegem et al., 2004). The idea that an intramolecular SH3–GK interaction is an important determinant of function in MAGUKs is well established; ablation of this interaction in Dlg generates a tumorigenic phenotype of larval imaginal discs in *Drosophila* (Woods et al., 1996); its disruption in PSD-95 inhibits the clustering of $K_V1.4$ potassium channels (Shin et al., 2000). Classically, the cis SH3–GK interaction in MAGUKs is envisioned as having an autoinhibitory role by preventing the two motifs from interacting in trans with other proteins (Masuko et al., 1999; McGee and Bredt, 1999; Nix et al., 2000; Shin et al., 2000; Seabold et al., 2003). Specific cellular signals can break the cis SH3–GK interaction, permitting the SH3 and GK domains to engage with other ligand-binding sites. For example, a trans interaction between the PSD-95 GK domain and the SH3 domain of another MAGUK, NE-dlg, is normally prevented by an intramolecular interaction, but can be turned on by Ca^{2+}-calmodulin (Masuko et al., 1999). In this regime, the SH3–GK interaction essentially behaves as an ON–OFF molecular switch. This behavior is analogous to what we find for $Ca_V\beta$ in that when the SH3–GK interaction is ablated, functional modulation of α_1 is lost. By contrast, the finding that finer adjustments of the $Ca_V\beta$ SH3–GK module can preferentially modulate distinct functions is a new twist on the classical conception. It will be interesting to determine whether analogous regulatory paradigms exist in other MAGUK proteins. Overall, the $Ca_V\beta$ SH3–GK module is distinguished from those of MAGUKs by having a precisely defined binding partner (namely the α_1 subunit) and functional signature (channel trafficking and gating modulation). Hence, further mechanistic understanding into the Ca^{2+} channel α_1–β interaction structure–function could yield new insights into the functional operation of the widely conserved SH3–GK structural module.

REFERENCES

Anderson, J.M. 1996. Cell signalling: MAGUK magic. *Curr. Biol.* 6:382–384.

Bichet, D., V. Cornet, S. Geib, E. Carlier, S. Volsen, T. Hoshi, Y. Mori, and M. De Waard. 2000. The I-II loop of the Ca^{2+} channel α_1 subunit contains an endoplasmic reticulum retention signal antagonized by the β subunit. *Neuron.* 25:177–190.

Birnbaumer, L., N. Qin, R. Olcese, E. Tareilus, D. Platano, J. Costantin, and E. Stefani. 1998. Structures and functions of calcium channel β subunits. *J. Bioenerg. Biomembr.* 30:357–375.

Brice, N.L., N.S. Berrow, V. Campbell, K.M. Page, K. Brickley, I. Tedder, and A.C. Dolphin. 1997. Importance of the different β subunits in the membrane expression of the α_{1A} and α_2 calcium channel subunits: studies using a depolarization-sensitive α_{1A} antibody. *Eur. J. Neurosci.* 9:749–759.

Canti, C., A. Davies, N.S. Berrow, A.J. Butcher, K.M. Page, and A.C. Dolphin. 2001. Evidence for two concentration-dependent processes for β-subunit effects on α_{1B} calcium channels. *Biophys. J.* 81:1439–1451.

Catterall, W.A. 2000. Structure and regulation of voltage-gated Ca^{2+} channels. *Annu. Rev. Cell Dev. Biol.* 16:521–555.

Chen, Y., M. Li, Y. Zhang, L. He, Y. Yamada, A. Fitzmaurice, Y. Shen, H. Zhang, L. Tong, and J. Yang. 2004. Structural basis of the α_1-β subunit interaction of voltage-gated Ca^{2+} channels. *Nature.* 429: 675–680.

Chien, A.J., X. Zhao, R.E. Shirokov, T.S. Puri, C.F. Chang, D. Sun, E. Rios, and M.M. Hosey. 1995. Roles of a membrane-localized β subunit in the formation and targeting of functional L-type Ca^{2+} channels. *J. Biol. Chem.* 270:30036–30044.

Colecraft, H.M., B. Alseikhan, S.X. Takahashi, D. Chaudhuri, S. Mittman, V. Yegnasubramanian, R.S. Alvania, D.C. Johns, E. Marban, and D.T. Yue. 2002. Novel functional properties of Ca^{2+} channel β subunits revealed by their expression in adult rat heart cells. *J. Physiol.* 541:435–452.

Craven, S.E., and D.S. Bredt. 1998. PDZ proteins organize synaptic signaling pathways. *Cell.* 93:495–498.

De Waard, M., M. Pragnell, and K.P. Campbell. 1994. Ca^{2+} channel regulation by a conserved β subunit domain. *Neuron.* 13:495–503.

Dolphin, A.C. 2003. β subunits of voltage-gated calcium channels. *J. Bioenerg. Biomembr.* 35:599–620.

Erickson, M.G., B.A. Alseikhan, B.Z. Peterson, and D.T. Yue. 2001. Preassociation of calmodulin with voltage-gated Ca^{2+} channels revealed by FRET in single living cells. *Neuron.* 31:973–985.

Erickson, M.G., H. Liang, M.X. Mori, and D.T. Yue. 2003. FRET two-hybrid mapping reveals function and location of L-type Ca^{2+} channel CaM preassociation. *Neuron.* 39:97–107.

Ertel, E.A., K.P. Campbell, M.M. Harpold, F. Hofmann, Y. Mori, E. Perez-Reyes, A. Schwartz, T.P. Snutch, T. Tanabe, L. Birnbaumer, et al. 2000. Nomenclature of voltage-gated calcium channels. *Neuron.* 25:533–535.

Funke, L., S. Dakoji, and D.S. Bredt. 2004. Membrane-associated guanylate kinases regulate adhesion and plasticity at cell junctions. *Annu. Rev. Biochem.* 74:219–245.

Gao, T., A.J. Chien, and M.M. Hosey. 1999. Complexes of the α_{1C} and β subunits generate the necessary signal for membrane targeting of class C L-type calcium channels. *J. Biol. Chem.* 274:2137–2144.

Gerhardstein, B.L., T. Gao, M. Bunemann, T.S. Puri, A. Adair, H. Ma, and M.M. Hosey. 2000. Proteolytic processing of the C terminus of the α_{1C} subunit of L-type calcium channels and the role of a proline-rich domain in membrane tethering of proteolytic fragments. *J. Biol. Chem.* 275:8556–8563.

Gerster, U., B. Neuhuber, K. Groschner, J. Striessnig, and B.E. Flucher. 1999. Current modulation and membrane targeting of the calcium channel α_{1C} subunit are independent functions of

the β subunit. *J. Physiol.* 517:353–368.

Hullin, R., I.F.Y. Khan, S. Wirtz, P. Mohacsi, G. Varadi, A. Schwartz, and S. Herzig. 2003. Cardiac L-type calcium channel β subunits expressed in human heart have differential effects on single channel characteristics. *J. Biol. Chem.* 278:21623–21630.

Maltez, J.M., D.A. Nunziato, J. Kim, and G.S. Pitt. 2005. Essential Ca$_V$β modulatory properties are AID-independent. *Nat. Struct. Mol. Biol.* 12:372–377.

Masuko, N., A. Makino, H. Kuwahara, K. Fukunaga, T. Suso, N. Araki, H. Yamamoto, Y. Yamada, E. Miyamoto, and H. Saya. 1999. Interaction of NE-dlg/SAP102, a neuronal and endocrine tissue-specific membrane-associated guanylate kinase protein, with calmodulin and PSD-95/SAP90. *J. Biol. Chem.* 274:5782–5790.

McGee, A.W., and D.S. Bredt. 1999. Identification of an intramolecular interaction between the SH3 and guanylate kinase domains of PSD-95. *J. Biol. Chem.* 274:17431–17436.

McGee, A.W., S.R. Dakoji, O. Olsen, D.S. Bredt, W.A. Lim, and K.E. Prehoda. 2001. Structure of the SH3-guanylate kinase module from PSD-95 suggests a mechanism for regulated assembly of MAGUK scaffolding proteins. *Mol. Cell.* 8:1291–1301.

McGee, A.W., D.A. Nunziato, J.M. Maltez, K.E. Prehoda, G.S. Pitt, and D.S. Bredt. 2004. Calcium channel function regulated by the SH3-GK module in β subunits. *Neuron.* 42:89–99.

Nix, S.L., A.H. Chisti, J.M. Anderson, and Z. Walther. 2000. hCASK and hDlg associate in epithelia, and their src homolgy 3 and guanylate kinase domains participate in both intramolecular and intermolecular interactions. *J. Biol. Chem.* 275:41192–41200.

Opatowsky, Y., O. Chomsky-Hecht, M.G. Kang, K.P. Campbell, and J.A. Hirsch. 2003. The voltage-dependent calcium channel β subunit contains two stable interacting domains. *J. Biol. Chem.* 278:52323–52332.

Opatowsky, Y., C.-C. Chen, K.P. Campbell, and J.A. Hirsch. 2004. Structural analysis of the voltage-dependent calcium channel β subunit functional core and its complex with the α$_1$ interaction domain. *Neuron.* 42:387–399.

Perez-Reyes, E., A. Castellano, H.S. Kim, P. Bertrand, E. Baggstrom, A.E. Lacerda, X.Y. Wei, and L. Birnbaumer. 1992. Cloning and expression of a cardiac/brain β subunit of the L-type calcium channel. *J. Biol. Chem.* 267:1792–1797.

Pragnell, M., M. De Waard, Y. Mori, T. Tanabe, T.P. Snutch, and K.P. Campbell. 1994. Calcium channel β-subunit binds to a conserved motif in the I-II cytoplasmic linker of the α$_1$-subunit. *Nature.* 368:67–70.

Seabold, G.K., A. Burette, I.A. Lim, R.J. Weinberg, and J.W. Hell. 2003. Interaction of the tyrosine kinase Pyk2 with the *N*-methyl-D-aspartate receptor complex via the Src homology 3 domains of PSD-95 and SAP102. *J. Biol. Chem.* 278:15040–15048.

Shin, H., Y.-P. Hsueh, E. Kim, and M. Sheng. 2000. An intramolecular interaction between Src homology 3 domain and guanylate kinase-like domain required for channel clustering by postsynaptic density-95/SAP 90. *J. Neurosci.* 20:3580–3587.

Singer, D., M. Biel, I. Lotan, V. Flockerzi, F. Hofmann, and N. Dascal. 1991. The roles of the subunits in the function of the calcium channel. *Science.* 253:1553–1557.

Stotz, S.C., and G.W. Zamponi. 2001. Structural determinants of fast inactivation of high voltage-activated Ca^{2+} channels. *Trends Neurosci.* 24:176–181.

Takahashi, S.X., S. Mittman, and H.M. Colecraft. 2003. Distinctive modulatory effects of five human auxiliary β$_2$ subunit splice variants on L-type calcium channel gating. *Biophys. J.* 84:3007–3021.

Takahashi, S.X., J. Miriyala, and H.M. Colecraft. 2004. Membrane-associated guanylate kinase-like properties of β subunits required for modulation of voltage-dependent Ca^{2+} channels. *Proc. Natl. Acad. Sci. USA.* 101:7193–7198.

Tavares, G.A., E.H. Panepucci, and A.T. Brunger. 2001. Structural characterization of the intramolecular interaction between the SH3 and guanylate kinase domains of PSD-95. *Mol. Cell.* 8:1313–1325.

Tsien, R.W., and R.Y. Tsien. 1990. Calcium channels, stores and oscillations. *Annu. Rev. Cell Biol.* 6:715–760.

Van Petegem, F., K.A. Clark, F.C. Chatelain, and D.L. Minor. 2004. Structure of a complex between a voltage-gated calcium channel β-subunit and an α-subunit domain. *Nature.* 429:671–675.

Walker, D., and M. De Waard. 1998. Subunit interaction sites in voltage-dependent Ca^{2+} channels: role in channel function. *Trends Neurosci.* 21:148–154.

Wei, S.K., H.M. Colecraft, C.D. DeMaria, B.Z. Peterson, R. Zhang, T.A. Kohout, T.B. Rogers, and D.T. Yue. 2000. Ca^{2+} channel modulation by recombinant auxiliary β subunits expressed in young adult heart cells. *Circ. Res.* 86:175–184.

Wei, X., A. Neely, A.E. Lacerda, R. Olcese, E. Stefani, E. Perez-Reyes, and L. Birnbaumer. 1994. Modification of Ca^{2+} channel activity by deletions at the carboxyl terminus of the cardiac α$_1$ subunit. *J. Biol. Chem.* 269:1635–1640.

Woods, D.F., C. Hough, D. Peel, G. Callaini, and P.J. Bryant. 1996. Dlg protein is required for junction structure, cell polarity, and proliferation control in *Drosophila* epithelia. *J. Cell Biol.* 134:1469–1482.

Young, K., S. Lin, L. Sun, E. Lee, M. Modi, S. Hellings, M. Husbands, B. Ozenberger, and R. Franco. 1998. Identification of a calcium channel modulator using a high throughput yeast two-hybrid screen. *Nat. Biotechnol.* 16:946–950.

Yue, D.T. 2004. The dawn of high-resolution structure for the queen of ion channels. *Neuron.* 42:357–359.